







Cite this: *Biomater. Sci.*, 2023, **11**, 1311

Received 29th October 2022,
Accepted 22nd January 2023

DOI: 10.1039/d2bm01763f

rsc.li/biomaterials-science

Facile fabrication of two-dimensional iodine nanosheets for antibacterial therapy†

Yingmin Ye,^{a,b} Yanmin Wang,^{a,b} Kai Zhang,^{a,b}  *^{a,b} Wei Guo,^{a,b} Tianyu Kong,^{a,b} Xiaokang Ding,^{a,b}  Nana Zhao  *^{a,b} and Fujian Xu  *^{a,b}

Herein, we report a facile approach for the preparation of two-dimensional iodine nanosheets (2D iodine NSs) with good stability and high biocompatibility via an aqueous solvent-assisted ultrasonic route. Due to the large specific surface area of the 2D morphology, iodine NSs effectively interact with bacterial membranes and destroy bacterial integrity, as well as further damaging intracellular DNA, showing prominent antibacterial activity against *S. aureus* *in vitro* and *in vivo*.

Pathogenic microorganisms such as bacteria, fungi, and viruses represent a serious threat to public health, causing millions of deaths worldwide.^{1–3} In the past decades, the appearance of antibiotics has contributed to saving millions of lives as their administration is a major and effective strategy to treat infectious diseases.^{4,5} However, these antibiotic-mediated therapeutic methods have been unsatisfactory with the emerging pathogenic infections induced by the spread of drug-resistant bacteria, which has become an issue of increasing concern.^{6,7} Thus, the discovery and development of new antimicrobial agents and alternative strategies to overcome bacterial resistance are critical. As an essential trace element for human health, iodine is one of the most commonly used disinfectants in clinical practice. It shows great potential in the treatment of infected wounds due to its good biocompatibility, high efficiency, broad spectrum, and low cost.⁸ Notably, iodine-containing antimicrobial agents have been verified to exhibit irreversible and nonspecific damage to microorganism cells, and can effectively avoid further spread of drug-resistant bacteria for antibacterial therapy.^{9,10} However, the poor solubi-

lity and easy volatility of iodine monomers severely impede its biological application.¹¹ Therefore, it is significant to develop new iodine-based antimicrobial agents with good stability and solubility, less toxicity, and effective antibacterial activity to treat bacterial infections.

Generally, polyvinylpyrrolidone (PVP) is employed as a stabilizer to absorb and stabilize iodine due to its ability to complex with iodine (PVP-I).^{12–14} Tremendous research works have demonstrated that PVP-I-containing implants could effectively prevent and treat post-operative infection after orthopedic surgery with no obvious cytotoxicity or adverse reactions.^{15,16} Recently, the *in situ* modification of iodine on the surface of titanium (Ti-I₂) was found to significantly promote the antibacterial properties of these antibacterial systems.¹⁷ Metal-organic frameworks (MOFs) as advanced drug delivery carriers have been widely employed to load and deliver iodine for antibacterial treatment.^{18,19} However, the insufficient loading capacity and inadequate release of iodine severely impair their antibacterial potency and thus hinder their further clinical applications. Therefore, it is desirable to fabricate new carrier-free iodine-based antimicrobial agents with good antibacterial activity.

The advent of nanotechnology has inspired the emergence of versatile antimicrobial agents, and numerous observations suggest that the physical parameters of nanomaterials, such as size and morphology, show significant influences on the bioavailability of antimicrobial nanosystems.^{20,21} Two-dimensional (2D) nanomaterials, carrying unique and specific morphologies, possess a much larger specific surface area,²² which not only exposes more active sites to improve their bio-catalytic performance but also increases the interaction area of nanomaterials and cells to facilitate damage to bacterial integrity.²³ Moreover, the ultra-thin property can enable physical cutting of bacterial membranes to enhance the antibacterial activity.^{24–26} For instance, our group reported 2D Cu-MOF nanosheets (NSs) for reactive oxygen species (ROS)-mediated antibacterial treatment. The higher specific surface area of 2D Cu-MOF NSs provided a high density of Cu²⁺/Cu⁺ surface

^aKey Laboratory of Biomedical Materials of Natural Macromolecules (Beijing University of Chemical Technology, Ministry of Education), Beijing Laboratory of Biomedical Materials, Beijing University of Chemical Technology, Beijing, 100029, China. E-mail: zzhangkai@sina.com, zhaonn@mail.buct.edu.cn, xufj@mail.buct.edu.cn

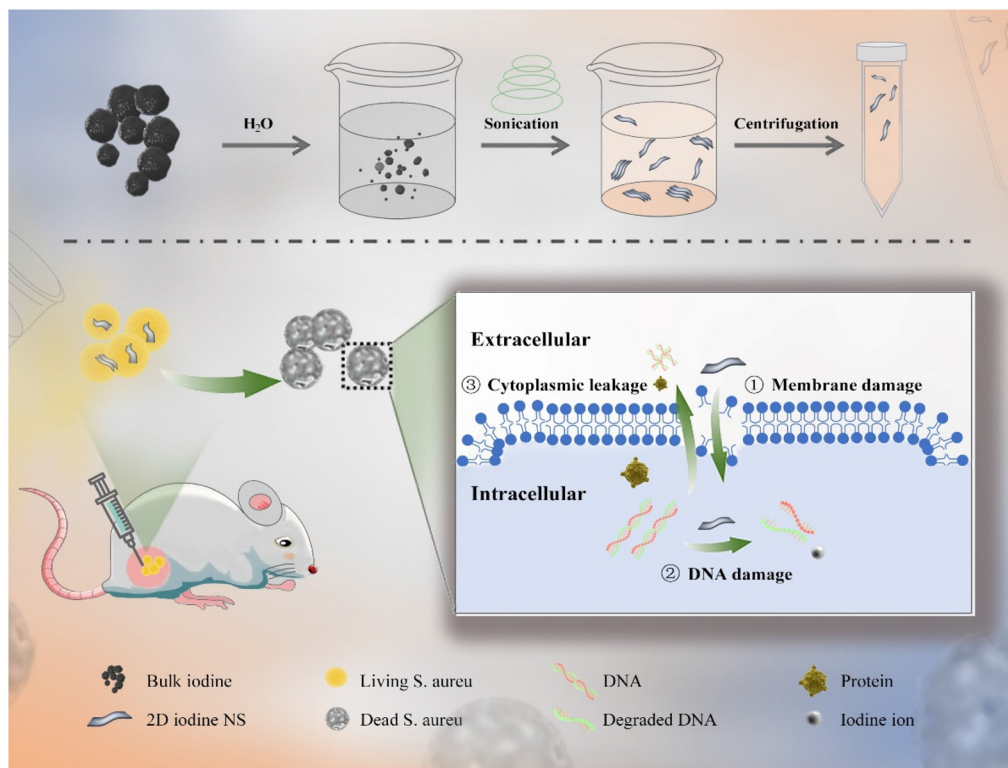
^bCollege of Materials Science and Engineering, Beijing University of Chemical Technology, Beijing, 100029, China

† Electronic supplementary information (ESI) available. See DOI: <https://doi.org/10.1039/d2bm01763f>

active sites to oxidize the proteins and lipids on the bacterial surface, and accelerate the diffusion rate of ROS, resulting in the enhancement of antibacterial performance. However, the inevitable leakage of Cu^{2+} ions induced the potential biotoxicity of Cu-MOF NSs, severely limiting their applications.²⁷ Thus, it is desirable to develop a 2D iodine antimicrobial platform with high antibacterial activity and good biosecurity.

In this work, we proposed a facile approach for the preparation of 2D iodine nanosheets (NSs) by exfoliating bulk iodine *via* an aqueous solvent-assisted ultrasonic route in an ice bath (Scheme 1).²⁸ By controlling the ultrasonic conditions, bulk iodine could be converted into multi- and monolayer iodine NSs, and the thickness of the resultant iodine NSs was observed using atomic force microscopy (AFM) analysis. The iodine NSs exhibited good solubility and stability in an aqueous solution. Taking advantage of the enhanced interaction area between 2D NSs and bacterial cells, the iodine NSs could effectively interact with the bacterial membranes and damage the integrity of bacteria, inducing the outflow of cytoplasm and biological molecules and further damage to the intracellular DNA. The iodine NSs showed prominent antibacterial activity against *Staphylococcus aureus* (*S. aureus*) *in vitro*. The results of bioluminescence imaging (BLI) and colony count demonstrate that the iodine NSs could effectively combat *S. aureus in vivo* and facilitate the recovery of abscess tissue. Additionally, the 2D iodine NSs exhibited high biocompatibility, providing a promising nanoplatform for clinical antibacterial treatment.

2D iodine NSs were synthesized from bulk iodine through ultrasonic treatment in an aqueous solvent. Bulk iodine was a dark grey spherical particle with metallic luster (Fig. S1[†]), which was insoluble in pure water (Fig. S2[†]). After receiving de-ionized water-assisted ultrasonic treatment, a brownish-yellow solution was obtained (Fig. S3[†]). The transmission electron microscopy (TEM) images showed the successful fabrication of ultrathin iodine NSs with planar topology (Fig. 1A). The observation of the dark-field TEM image (Fig. 1B) and the energy dispersive spectroscopy (EDS) element mapping of I revealed the distribution of elemental iodine on 2D iodine NSs (Fig. 1C). As shown in Fig. 1D, X-ray photoelectron spectroscopy (XPS) was further employed to verify the surface state of 2D iodine NSs. The binding energy peaks of $\text{I } 3d_{3/2}$ and $\text{I } 3d_{5/2}$ in the structure of 2D iodine NSs were located at 618.8 and 630.2 eV, respectively, showing a difference of 11.4 eV, which indicated that the valence state of the iodine element was I (0). The topographic height of iodine NSs was about 1.29 nm based on the AFM images and the height profiles (Fig. 1E and F). Furthermore, the photographs of the iodine NS solution showed that there was no significant change of color of the precipitate after 3 days (Fig. S4[†]). Additionally, no significant morphology changes of iodine NSs were observed after receiving the treatment of water, whereas the iodine NSs exhibited obvious degradation when they were incubated with the cell culture medium (Fig. S5[†]). These results demonstrated the good stability of iodine NSs *in vitro* and excellent biodegradability *in vivo*.



Scheme 1 Schematic illustration of the preparation procedure of the 2D iodine NSs by exfoliating bulk iodine through an aqueous solvent-assisted ultrasonic route in an ice bath and its antibacterial performance in combating *S. aureus in vivo*.

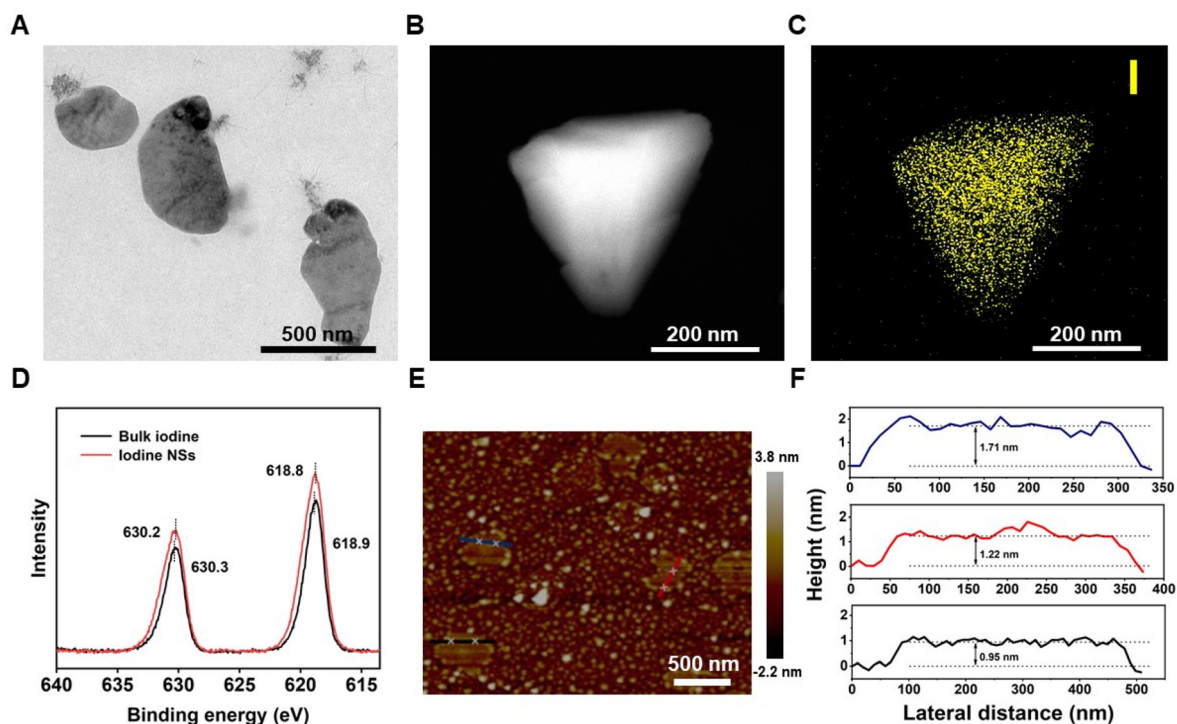


Fig. 1 Characterization of 2D iodine NSs. (A) TEM image. (B) Dark-field TEM image. (C) Elemental mapping of iodine. (D) XPS spectra of bulk iodine and iodine NSs. (E) AFM image. (F) Height profiles along the corresponding lines in (E).

As shown in Fig. 2, the antibacterial activity and the antibacterial mechanism of iodine NSs *in vitro* were investigated using *S. aureus* as an experimental model, a representative of Gram-positive bacteria. Firstly, the bacterial viability of *S. aureus* cultured with iodine NSs at different concentrations was determined by Cell Counting Kit-8 (CCK-8) assay (Fig. 2A). Along with the increase in iodine NS concentrations, the bacterial survival of *S. aureus* decreased, and *S. aureus* displayed a bacterial viability of 4.73% when the concentration of iodine NSs was $256 \mu\text{g mL}^{-1}$. Furthermore, the Live/Dead double-staining result of *S. aureus* is presented in Fig. 2B to visualize the distribution of live and dead bacteria after receiving the treatment of iodine NSs. A LIVE/DEAD™ BacLight™ Bacterial Viability Kit was employed to carry out this experiment, in which propidium iodide (PI) with enhanced red fluorescence only penetrated bacteria with damaged membranes, and the living bacteria were stained green with SYTO 9.²⁹ *S. aureus* treated with the iodine NSs showed high bacterial death ratios. These results demonstrated the good antibacterial activity of 2D iodine NSs in killing *S. aureus in vitro*.

To visually assess the capacity of iodine NSs to damage the bacterial membranes, we observed the morphologies of *S. aureus* after co-culture with the 2D iodine NSs by scanning electron microscopy (SEM) imaging. As shown in Fig. 2C, untreated *S. aureus* displayed an intact morphology and a smooth body. Once *S. aureus* was incubated with the iodine NSs, the membranes of the bacteria were rough and wrinkled, and the bacterial shape changed, indicating that the integrity

of *S. aureus* was effectively disrupted due to the interaction of the bacterial surface and 2D iodine NSs. The wrinkled and lysed cell walls, the disrupted integrity of bacteria, and the apparent leakage of the intracellular content from bacteria demonstrated that the 2D iodine NSs could effectively damage the integrity of the bacterial structure and further cause the leakage of the intracellular content, thus inducing bacterial death and achieving highly efficient antibacterial performance.

The antibacterial mechanism of 2D iodine NSs was further studied and discussed. Considering the high damage capacity of iodine NSs to the bacterial membranes and the apparent leakage of the intracellular content, we assumed that the iodine NSs could interact with intracellular biological components such as DNA, further accelerating bacterial death. The ability of iodine NSs to damage DNA within *S. aureus* was verified by agarose gel electrophoresis (Fig. 2D). Compared with the control group, no significantly bright bands could be observed in the groups of the DNA extracted from *S. aureus* treated with the iodine NSs. The phenomena were attributed to the highly effective interaction between the iodine NSs and intracellular DNA, and the iodine NSs attacked key nucleotides bearing thiol and amino groups, thereby damaging intrabacterial DNA or degrading it to smaller DNA fragments.³⁰ These results suggest that the iodine NSs could severely damage the DNA in the bacteria and accelerate bacterial death. The disruption of bacterial proteins by the iodine NSs was investigated by sodium dodecyl sulfate polyacrylamide gel electrophoresis (SDS-PAGE). As shown in Fig. S6,† the protein bands of bac-

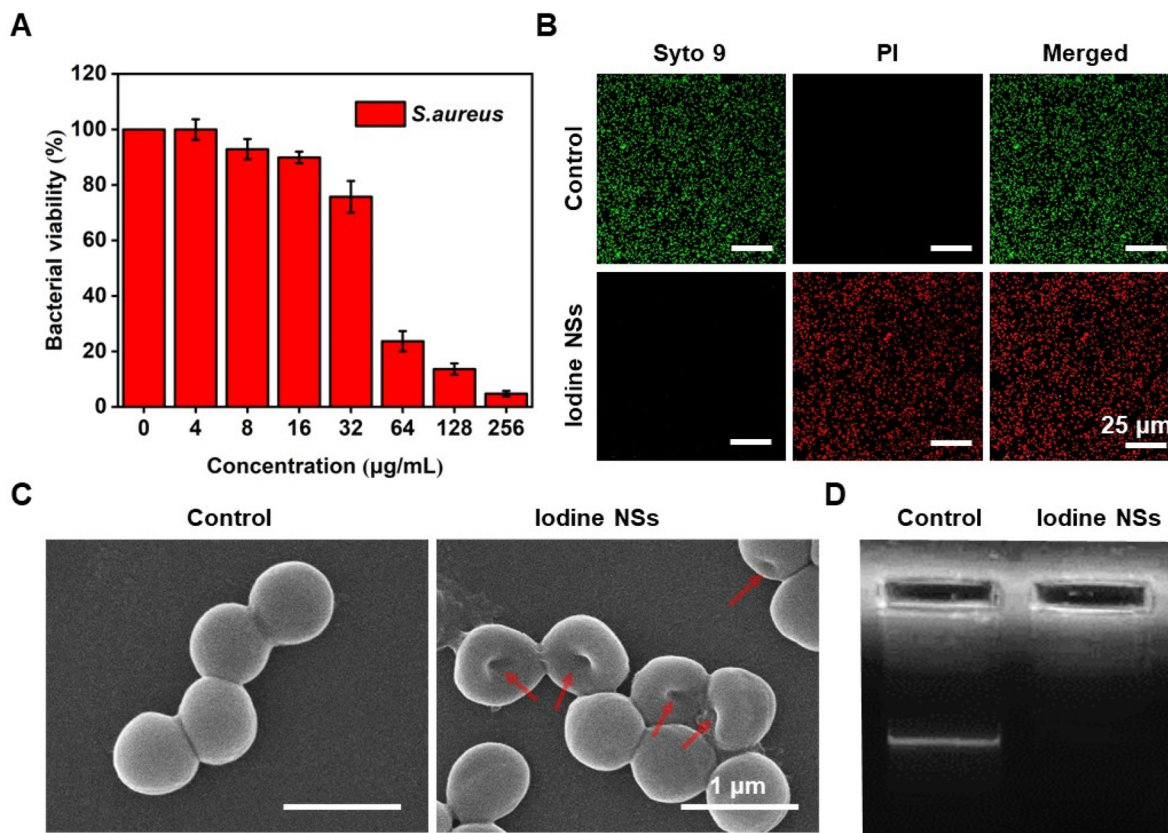


Fig. 2 Antibacterial performance of 2D iodine NSs *in vitro*. (A) Bacterial viability of *S. aureus* incubated with iodine NSs at different concentrations. (B) Representative CLSM images of *S. aureus* treated with iodine NSs and PBS (as control) *via* live/dead bacterial staining assay. The scale bar is 25 μm . (C) SEM images of *S. aureus* after the treatments with iodine NSs and PBS (as control), respectively. The scale bar is 1 μm . (D) Genomic DNA bands of *S. aureus* after the treatment with PBS (lane 1) and iodine NSs (lane 2) using agarose gel electrophoresis.

teria treated with the iodine NSs were lighter, demonstrating that the resultant iodine NSs could severely damage proteins in bacteria.

Therefore, the antibacterial mechanism of iodine NSs is mainly through the oxidation of unsaturated fatty acids and amino acids in bacterial cell membranes, leading to their denaturation and inactivation, further aggravating the destabilization of structural components on cell membranes, then oxidizing DNA and proteins in bacterial cells, and ultimately inducing bacterial death.

Inspired by the high antibacterial activity of iodine NSs *in vitro*, we investigated the antibacterial performance of the resultant 2D iodine NSs *in vivo* using bioluminescent *S. aureus*-infected mice as a model (Fig. 3A). The bioluminescence imaging (BLI) was performed to accurately quantify and visually monitor the antibacterial effect of iodine NSs. As shown in Fig. 3B and C, the obvious BLI signal could be observed for the control group, and along with the increase in the treatment time, the BLI signal intensities decreased, which might be ascribed to the immune self-clearance of the body. In contrast, the BLI signal of iodine NS-injected mice significantly decreased in two days, and the infection of *S. aureus* almost disappeared after 6-day treatment, displaying only

7.5% of bacteria remaining, which was lower than that of the phosphate buffered saline (PBS)-treated mice. These results indicated that the iodine NS-mediated antibacterial treatment could greatly decrease the bacterial burden of *S. aureus in vivo*.

The agar plate count of homogenized tissue dispersions from the infected sites of mice that received different treatments was also used to evaluate the antibacterial activity of iodine NSs *in vivo*. As shown in Fig. 3D, the bacterial colonies of *S. aureus* collected from the abscess sites of the PBS-treated mice were clearly observed on agar plates, whereas few *S. aureus* colonies appeared in the plate of the samples from the iodine NS-injected mice. Moreover, the *S. aureus*-infected tissues receiving different treatments were collected and stained with hematoxylin and eosin (H&E) to further investigate the anti-infective ability of iodine NSs. As shown in Fig. 3E, many inflammatory cells (red arrows) which were stained in blue could be observed in the infected tissue from the PBS-treated mice. In contrast, the iodine NS-treated group displayed normal morphological features with fewer inflammatory cells. These results further confirmed the high antibacterial performance of 2D iodine NSs and their negligible damage to normal tissues.

The biocompatibility of the 2D iodine NSs was systematically and carefully evaluated in this work. CCK-8 assay revealed

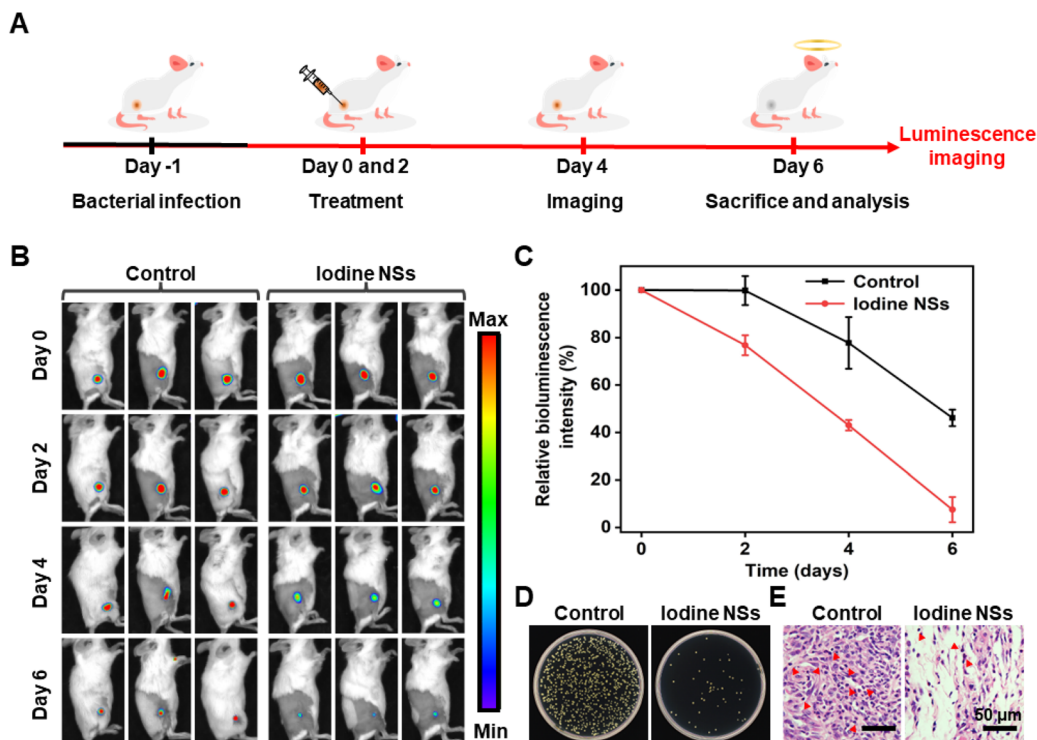


Fig. 3 Antibacterial performance of 2D iodine NSs *in vivo*. (A) Schematic diagram of the iodine NS-mediated and BLI-guided treatment procedure for combating *S. aureus* infection in living mice. Images of bioluminescence imaging (B) and representative bioluminescence signal intensity (C) of infected tissues injected with iodine NSs and PBS (as control). (D) Quantitative analysis of *S. aureus* colonies from infected sites of different groups. (E) H&E images of infected tissue were collected from different treatment groups after 6 days.

that the cell viabilities of L929 cells (mouse fibroblasts) were above 80% even if the concentration of iodine NSs was $200 \mu\text{g mL}^{-1}$, indicating the low cytotoxicity of iodine NSs (Fig. S7[†]). The effect of iodine NSs on red blood cells (RBCs) was also investigated by the hemolysis analysis method (Fig. S8[†]). No significant hemolytic phenomenon could be observed, and the hemolysis ratio was below the permissible limit (5%) along with an increase in the concentration of iodine NSs, showing negligible hemolytic activity of iodine NSs. These results suggested the good biocompatibility of iodine NSs *in vitro*.

Furthermore, the potential toxicity *in vivo* of the 2D iodine NSs was investigated *via* blood routine and biochemical indexes (Fig. S9[†]). The biochemical blood analysis was carried out on the mice receiving the injection of PBS (as control) and iodine NSs after six-day treatment. The blood routines including the levels of white blood cells (WBC), red blood cells (RBC), hemoglobin (HGB), hematocrit (HCT), mean corpuscular hemoglobin concentration (MCHC), mean corpuscular volume (MCV), and mean corpuscular hemoglobin (MCH) as the normal hematology parameters showed no abnormal changes after six days in comparison with those in the control group. The levels of urea nitrogen (BUN) as an indicator of renal function and alanine aminotransferase (ALT) as an indicator of liver function were also in the standard range, indicating no hepatic or renal toxicity of iodine NSs. Additionally, H&E staining of major organs, including the heart, liver,

spleen, lungs, and kidneys, showed no evident inflammation or noticeable signs of damage to the normal anatomical structures of organs (Fig. S10[†]). These results demonstrated that the resultant 2D iodine NSs had good biocompatibility *in vivo*, showing their potential for further clinical applications.

Conclusions

In summary, we proposed a facile approach for the preparation of 2D iodine NSs by exfoliating bulk iodine through an aqueous solvent-assisted ultrasonic route, and systematically explored its antibacterial performance *in vitro* and *in vivo*. Benefiting from the large specific surface area, the 2D iodine NSs could effectively interact with the surface of bacteria and directly destroy the integrity of bacteria due to the strong oxidation capability of iodine against cell membranes and proteins. Additionally, the iodine NSs could damage the DNA outflow from the bacterial cytoplasm, showing good antibacterial efficiency to combat *S. aureus in vitro*. Furthermore, using subcutaneous *S. aureus*-infected mice as a model, the *in vivo* experimental results demonstrated that the iodine NSs showed high antibacterial activity and elimination capacity of subcutaneous abscesses with good biosecurity. This work paved a new way for the facile preparation of iodine-based bac-

tericides, showing the efficient antibacterial performance of 2D iodine NSs with high application prospects in clinics.

Author contributions

All authors have approved the final version of the manuscript. Yingmin Ye: conceptualization, investigation, methodology, data curation, formal analysis, visualization, and writing – original draft. Yanmin Wang: methodology. Kai Zhang: conceptualization, investigation, methodology, visualization, writing – original draft, writing – review & editing, project administration, supervision, and funding acquisition. Wei Guo: methodology. Tianyu Kong: methodology and formal analysis. Xiaokang Ding: methodology and formal analysis. Nana Zhao: writing – review & editing, project administration, resources, supervision, and funding acquisition. Fujian Xu: writing – review & editing, project administration, resources, supervision, and funding acquisition.

Conflicts of interest

There are no conflicts to declare.

Acknowledgements

All animal procedures were performed in accordance with the Guidelines for Care and Use of Laboratory Animals of Peking Union Medical College and approved by the Animal Ethics Committee of Chinese Academy of Medical Sciences. This work was supported by the Beijing Natural Science Foundation (Grant No. 2214074), the National Key Research and Development Program of China (Grant No. 2022YFC2403200, 2022YFB3804600), the Science Fund for Creative Research Groups of the National Natural Science Foundation of China (52221006), the National Natural Science Foundation of China (Grant No. 52173271 and 51922022), the Beijing Outstanding Young Scientist Program (Grant No. BJJWZYJH01201910010024), the China Postdoctoral Science Foundation (Grant No. 2021T140044 and 2020M670110), the Beijing Municipal Science and Technology Project (No. Z191100006619099), and the Fundamental Research Funds for the Central Universities (Project No. ZY2201, BHYC1705A, and XK1802-2).

References

- 1 A. C. Fagre, L. E. Cohen, E. A. Eskew, M. Farrell, E. Glennon, M. B. Joseph, H. K. Frank, S. J. Ryan, C. J. Carlson and G. F. Albery, *Ecol. Lett.*, 2022, **25**, 1534–1549.
- 2 M. L. Ermini and V. Voliani, *ACS Nano*, 2021, **15**, 6008–6029.
- 3 Y. Wang, Y. Xu, X. Guo, L. Wang, J. Zeng, H. Qiu, Y. Tan, D. Chen, H. Zhao and Y. Gu, *Adv. Drug Delivery Rev.*, 2022, **183**, 114168.
- 4 F. Micoli, F. Bagnoli, R. Rappuoli and D. Serruto, *Nat. Rev. Microbiol.*, 2021, **19**, 287–302.
- 5 K. Lewis, *Cell*, 2020, **181**, 29–45.
- 6 C. Willyard, *Nature*, 2017, **543**, 15–15.
- 7 A. Lin, Y. Liu, X. Zhu, X. Chen, J. Liu, Y. Zhou, X. Qin and J. Liu, *ACS Nano*, 2019, **13**, 13965–13984.
- 8 Z. Miao, Y. Sun, Z. Tao, Y. Chen, Y. Ma, D. Zhu, X. Huang and Z. Zha, *Adv. Healthcare Mater.*, 2021, **10**, 2100722.
- 9 S. M. Andrabi, P. Singh, S. Majumder and A. Kumar, *Chem. Eng. J.*, 2021, **423**, 130219.
- 10 A.-N. Au-Duong and C.-K. Lee, *Mater. Sci. Eng., C*, 2017, **76**, 477–482.
- 11 Q. Borjihan, Z. Zhang, X. Zi, M. Huang, Y. Chen, Y. Zhang and A. Dong, *J. Hazard. Mater.*, 2020, **384**, 121305.
- 12 P. L. Bigliardi, S. A. L. Alsagoff, H. Y. El-Kafrawi, J.-K. Pyon, C. T. C. Wa and M. A. Villa, *Int. J. Surg.*, 2017, **44**, 260–268.
- 13 E. L. Papadopoulou, P. Valentini, F. Mussino, P. P. Pompa, A. Athanassiou and I. S. Bayer, *Chem. Eng. J.*, 2018, **347**, 19–26.
- 14 T. Gao, H. Fan, X. Wang, Y. Gao, W. Liu, W. Chen, A. Dong and Y.-J. Wang, *ACS Appl. Mater. Interfaces*, 2017, **9**, 25738–25746.
- 15 V. Pawar, H. Topkar and R. Srivastava, *Int. J. Biol. Macromol.*, 2018, **115**, 1131–1141.
- 16 W. Teng, Z. Zhang, Y. Wang, Y. Ye, E. Yinwang, A. Liu, X. Zhou, J. Xu, C. Zhou, H. Sun, F. Wang, L. Zhang, C. Cheng, P. Lin, Y. Wu, Z. Gou, X. Yu and Z. Ye, *Small*, 2021, **17**, 2102315.
- 17 T. Shirai, T. Shimizu, K. Ohtani, Y. Zen, M. Takaya and H. Tsuchiya, *Acta Biomater.*, 2011, **7**, 1928–1933.
- 18 X. Han, G. Boix, M. Balcerzak, O. H. Moriones, M. Cano-Sarabia, P. Cortés, N. Bastús, V. Puentes, M. Llagostera, I. Imaz and D. Maspocho, *Adv. Funct. Mater.*, 2022, **32**, 2112902.
- 19 S. Lu, X. Ren, T. Guo, Z. Cao, H. Sun, C. Wang, F. Wang, Z. Shu, J. Hao, S. Gui, C. Lei and J. Zhang, *Carbohydr. Polym.*, 2021, **267**, 118187.
- 20 J. A. Doolan, G. T. Williams, K. L. F. Hilton, R. Chaudhari, J. S. Fossey, B. T. Goult and J. R. Hiscock, *Chem. Soc. Rev.*, 2022, **51**, 8696–8755.
- 21 Y. Liu, L. Shi, L. Su, H. C. van der Mei, P. C. Jutte, Y. Ren and H. J. Busscher, *Chem. Soc. Rev.*, 2019, **48**, 428–446.
- 22 S. Liu, X. Pan and H. Liu, *Angew. Chem., Int. Ed.*, 2020, **59**, 5890–5900.
- 23 Z. Tu, G. Guday, M. Adeli and R. Haag, *Adv. Mater.*, 2018, **30**, 1706709.
- 24 J. Liu, R. S. Li, M. He, Z. Xu, L. Q. Xu, Y. Kang and P. Xue, *Biomaterials*, 2021, **277**, 121084.
- 25 X. Wang, X. Sun, T. Bu, Q. Wang, P. Jia, M. Dong and L. Wang, *Composites, Part B*, 2022, **229**, 109465.
- 26 N. Lin, P. Berton, C. Moraes, R. D. Rogers and N. Tufenkji, *Adv. Colloid Interface Sci.*, 2018, **252**, 55–68.

- 27 Z. Wang, W. Guo, K. Zhang, Y. Ye, Y. Wang, D. Sui, N. Zhao and F.-J. Xu, *Sci. China: Technol. Sci.*, 2022, **65**, 1052–1058.
- 28 M. Qian, Z. Xu, Z. Wang, B. Wei, H. Wang, S. Hu, L.-M. Liu and L. Guo, *Adv. Mater.*, 2020, **32**, 2004835.
- 29 L. Boulos, M. Prévost, B. Barbeau, J. Coallier and R. Desjardins, *J. Microbiol. Methods*, 1999, **37**, 77–86.
- 30 G. McDonnell and A. D. Russell, *Clin. Microbiol. Rev.*, 1999, **12**, 147–179.